Journal of Advances in Modeling Earth Systems

Supporting Information for

Impacts of sub-grid topographic representations on surface energy balance and boundary conditions in the E3SM Land Model

Dalei Hao[1], Gautam Bisht[1], Meng Huang[1], Po-Lun Ma[1], Teklu Tesfa[1], Wei-Liang Lee[2], Yu Gu[3], L. Ruby Leung[1]

[1]Atmospheric Sciences and Global Change Division, Pacific Northwest National Laboratory, Richland, WA, USA

[2]Research Center for Environmental Changes, Academia Sinica, Taipei, Taiwan

[3]Joint Institute for Regional Earth System Science and Engineering and Department of Atmospheric and Oceanic Sciences, University of California, Los Angeles, CA, USA

Corresponding author: Dalei Hao (dalei.hao@pnnl.gov)

Contents of this file

Introduction

The figures presented here are auxiliary information to support the conclusions made in the main text.

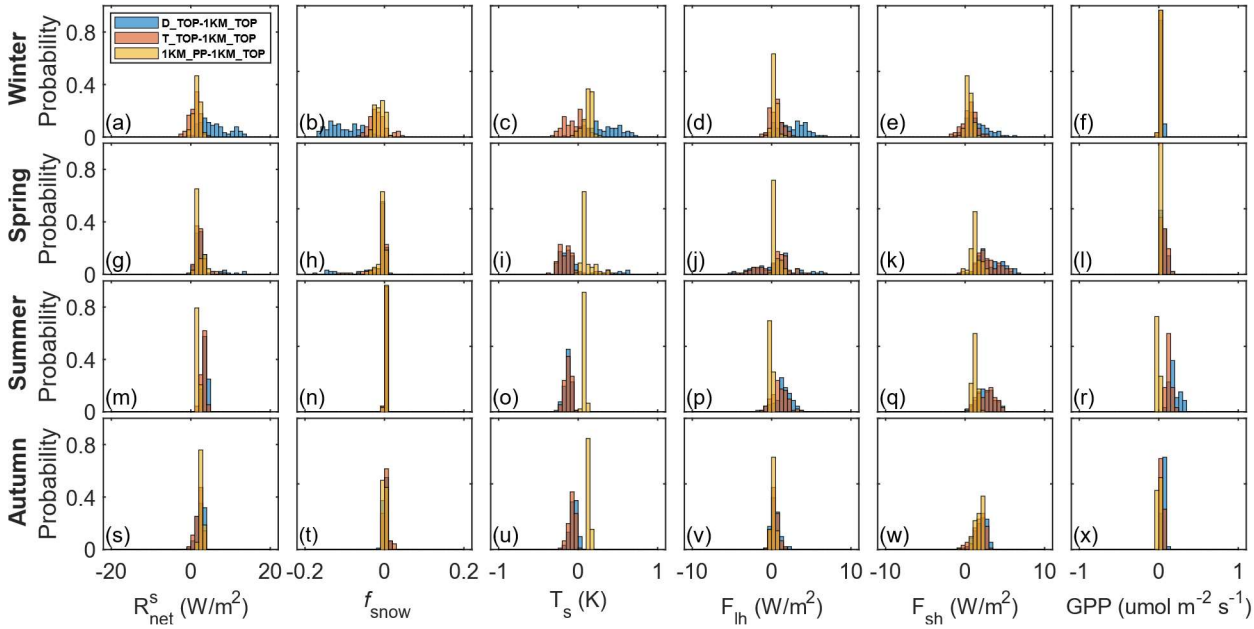

Figure S1. Statistical histograms of the *mean* differences in R_{net}^{s}, f_{snow}, $\mathrm{T_s}$, $\mathrm{F_{lh}}$, $\mathrm{F_{sh}}$ and GPP between different cases of G2 for different seasons. Here, the differences were calculated as the differences between other cases and 1KM_TOP case. The bar color is semi-transparent to show the overlapping regions.

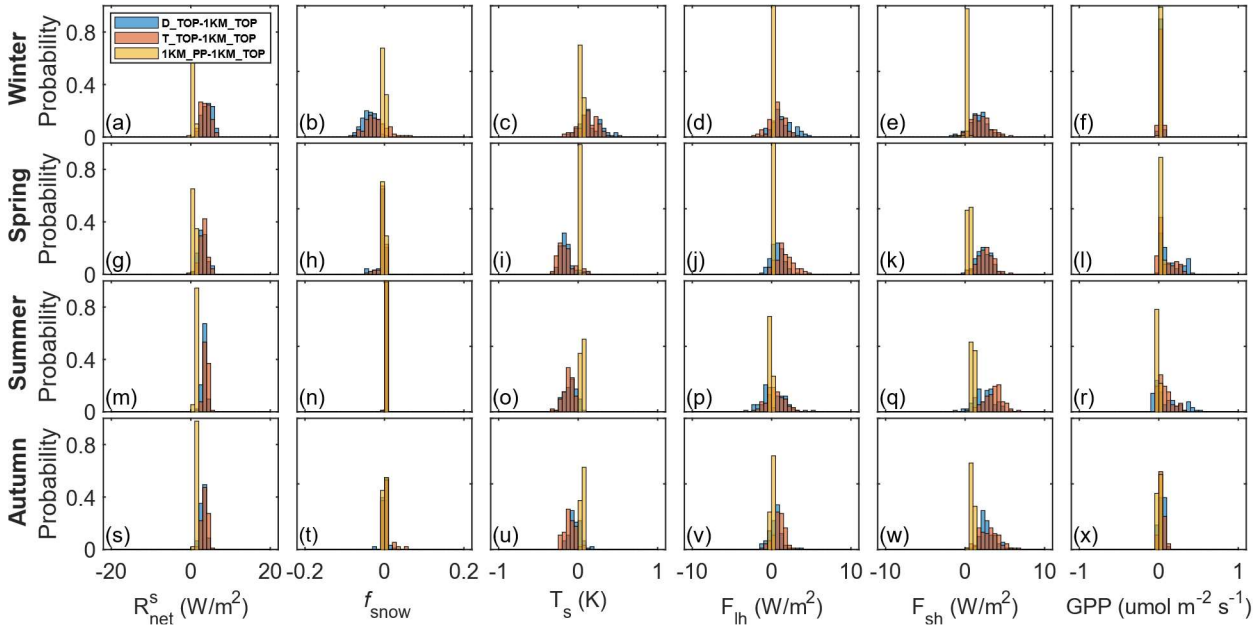

Figure S2. Same as Figure S1, except for G3.

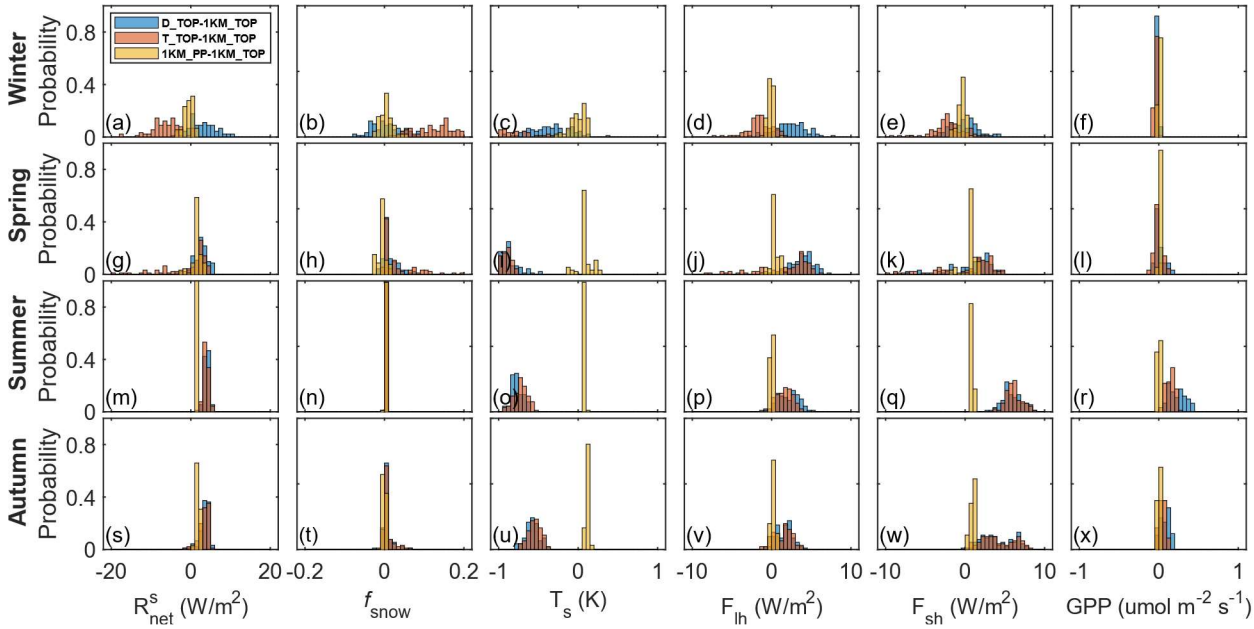

Figure S3. Same as Figure S1, except for G4.

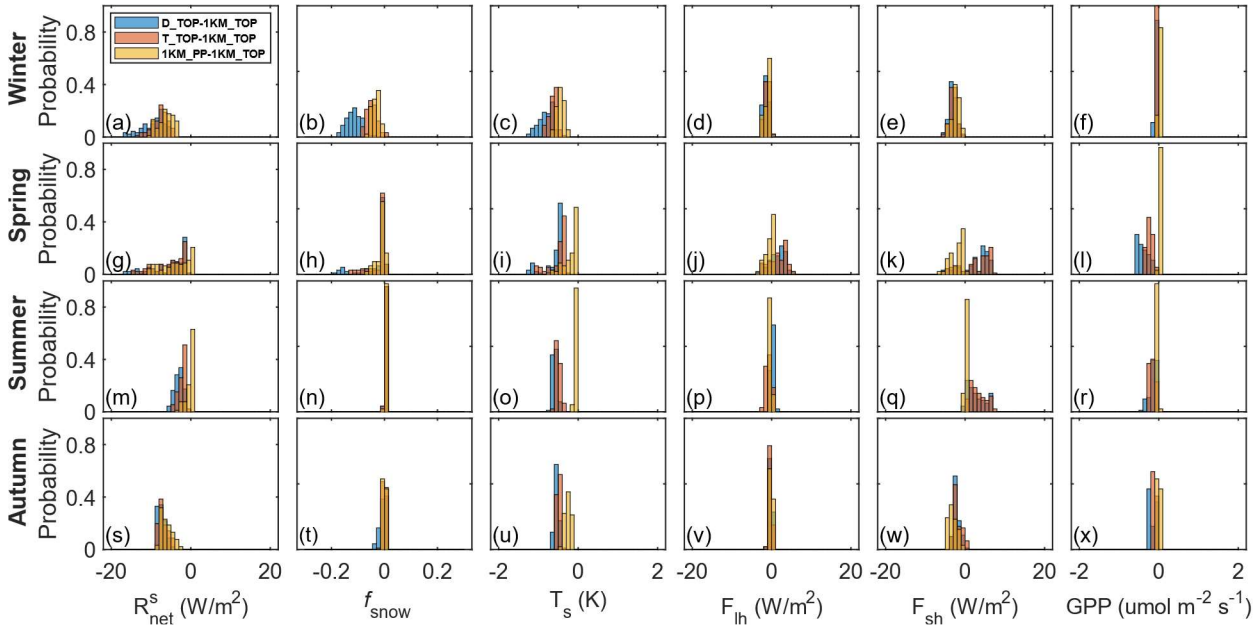

Figure S4. Same as Figure S1, except for *std* over G2.

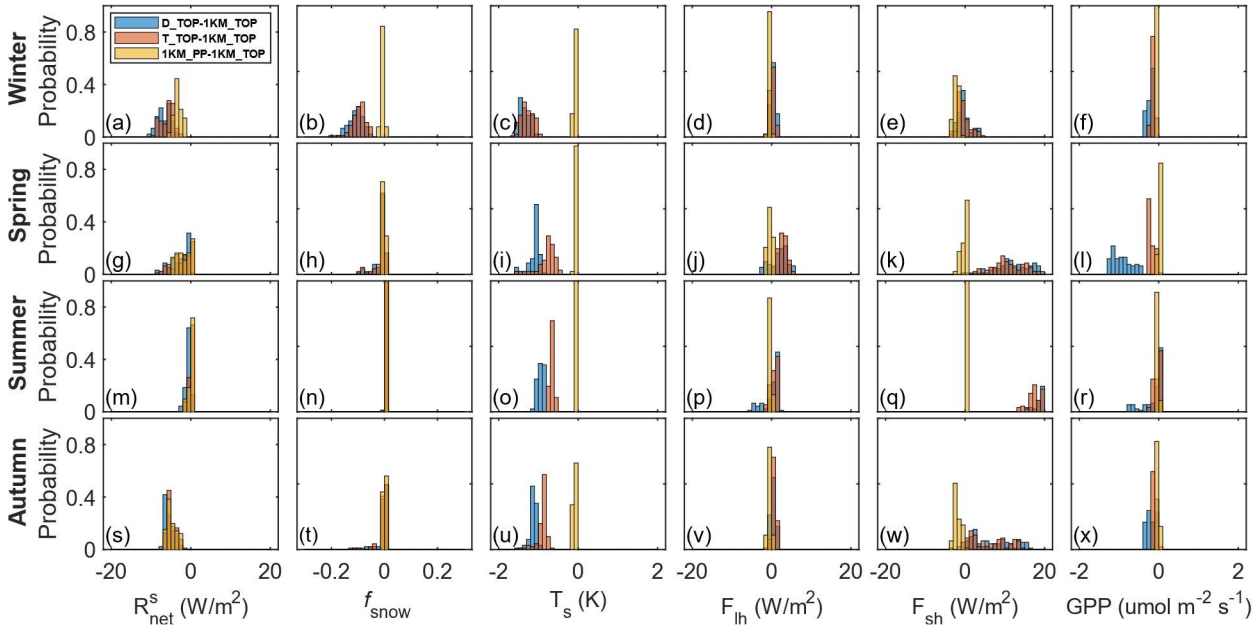

Figure S5. Same as Figure S1, except for *std* over G3.

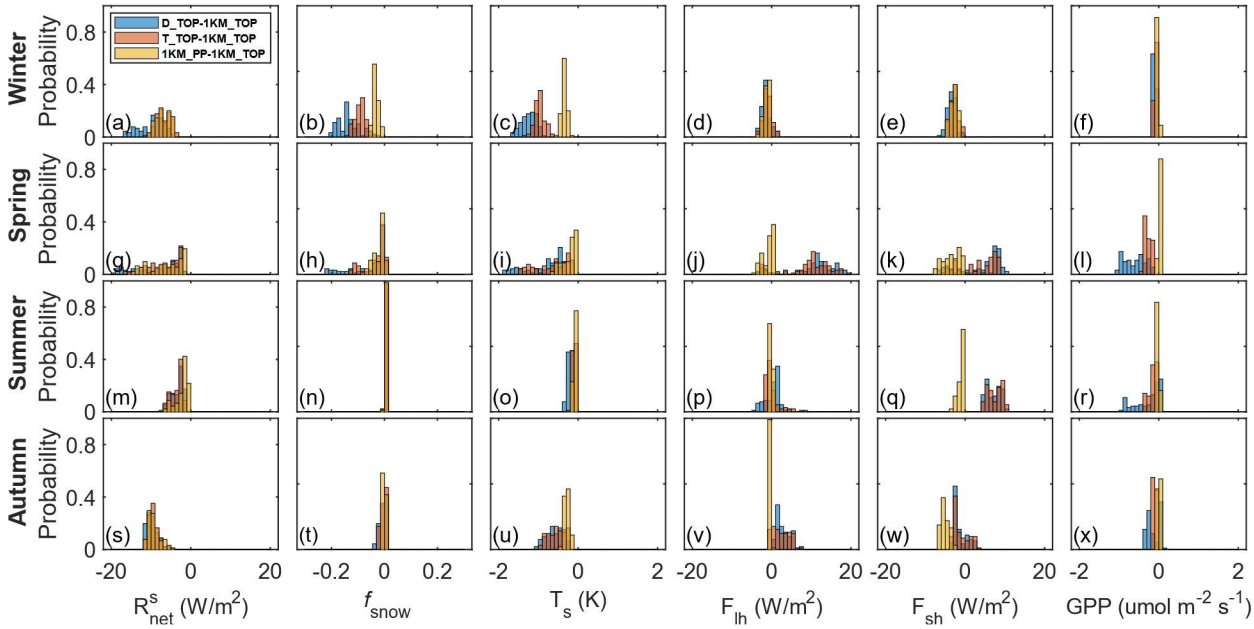

Figure S6. Same as Figure S1, except for *std* over G4.

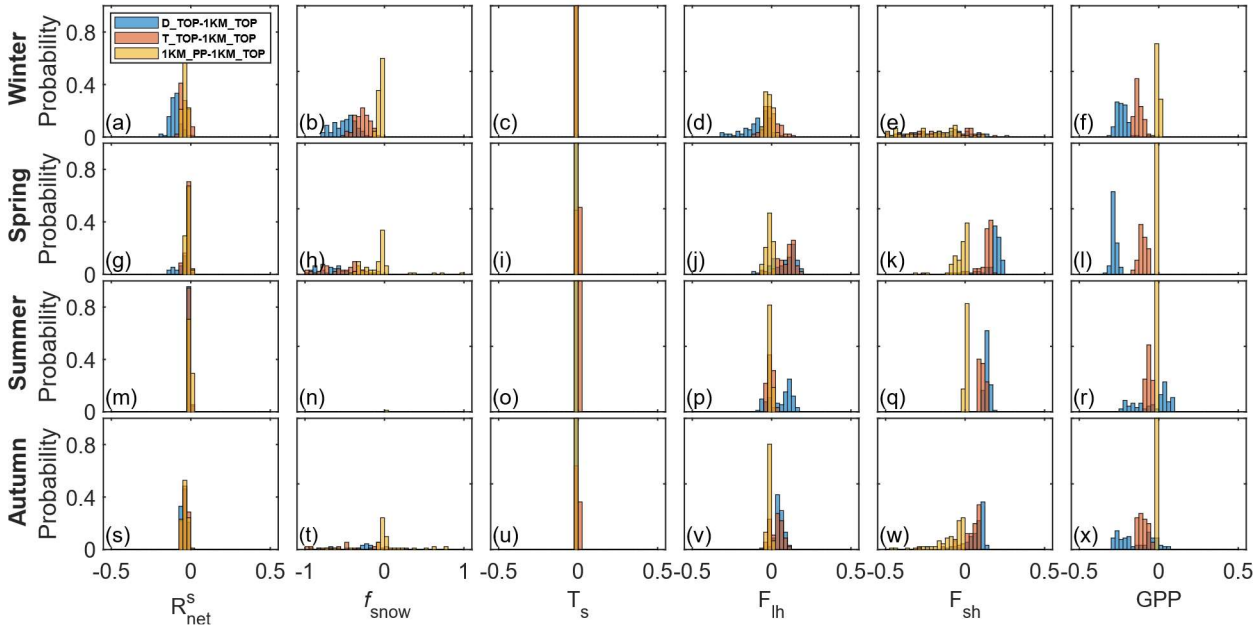

Figure S7. Same as Figure S1, except for *cv* over G1.

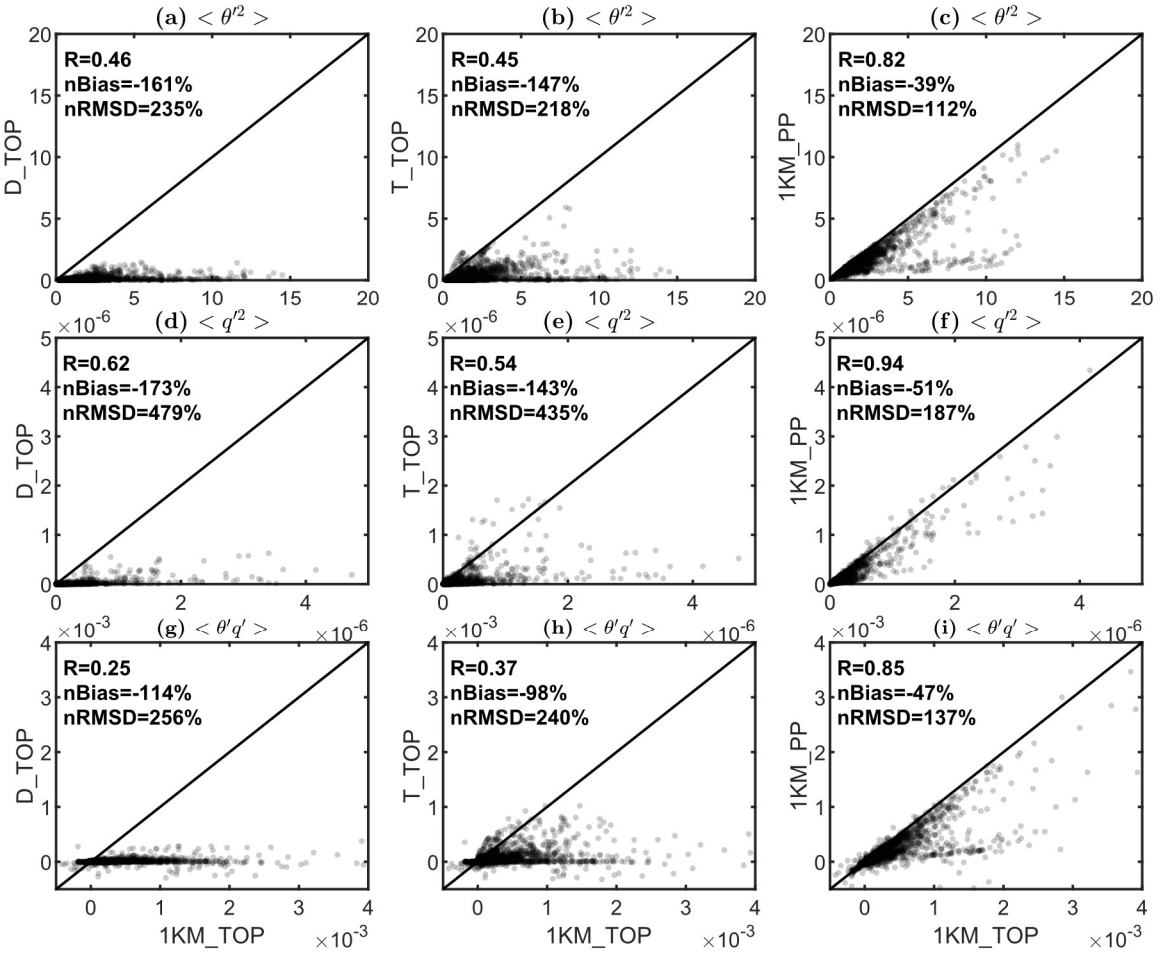

Figure 8. Comparisons of 1KM_TOP simulated (a-c) temperature variance ($\langle \theta'^2 \rangle$), (d-e) humidity variance ($\langle q'^2 \rangle$), and (g-i) temperature-humidity covariance ($\langle \theta' q' \rangle$) in winter (DJF) over G2 against simulated values from D_TOP, T_TOP and 1KM_PP model configurations. The (co-)variances were derived using the HET methods introduced in Section 2.4; and R, nBias and nRMSD were shown in each sub-plot.

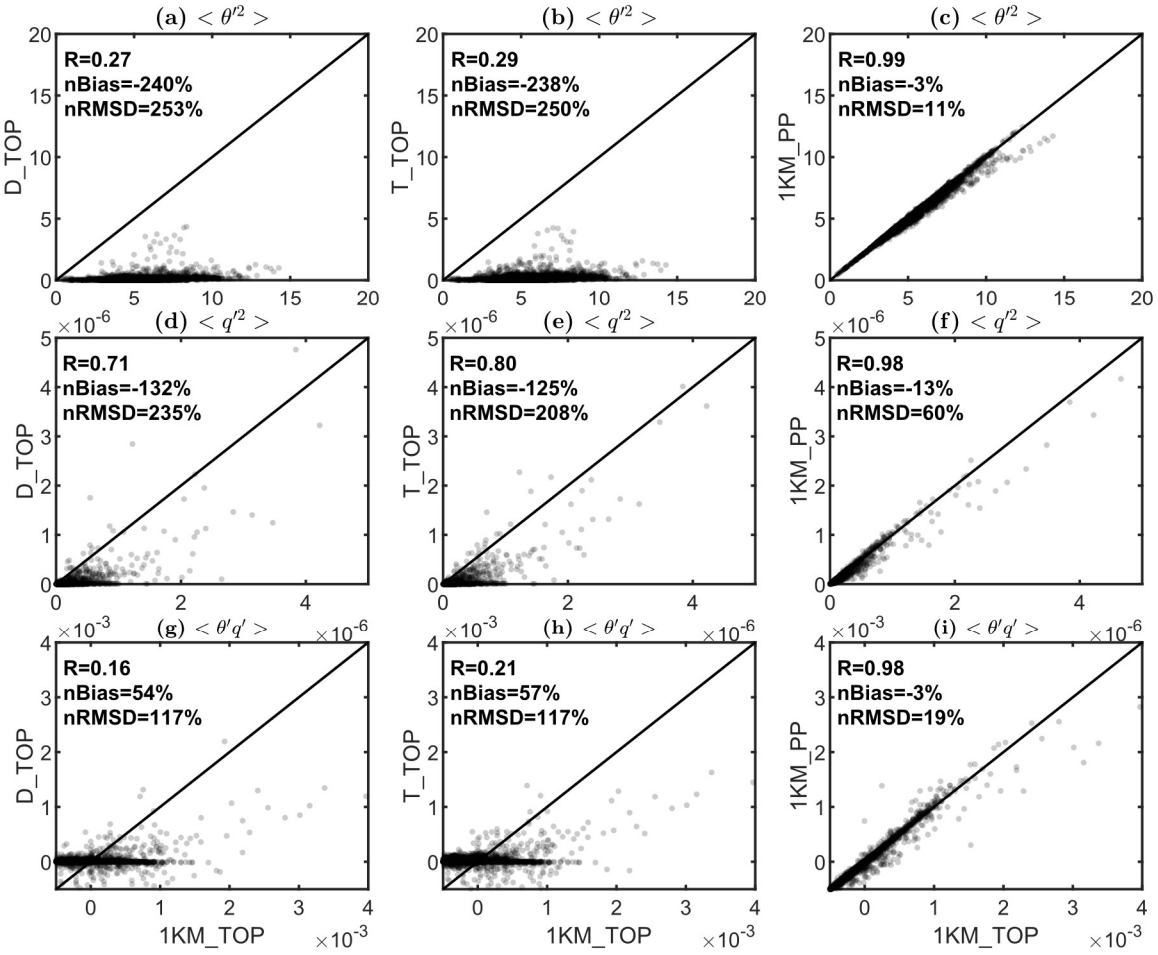

Figure S9. Same as Figure S8, except for G3.

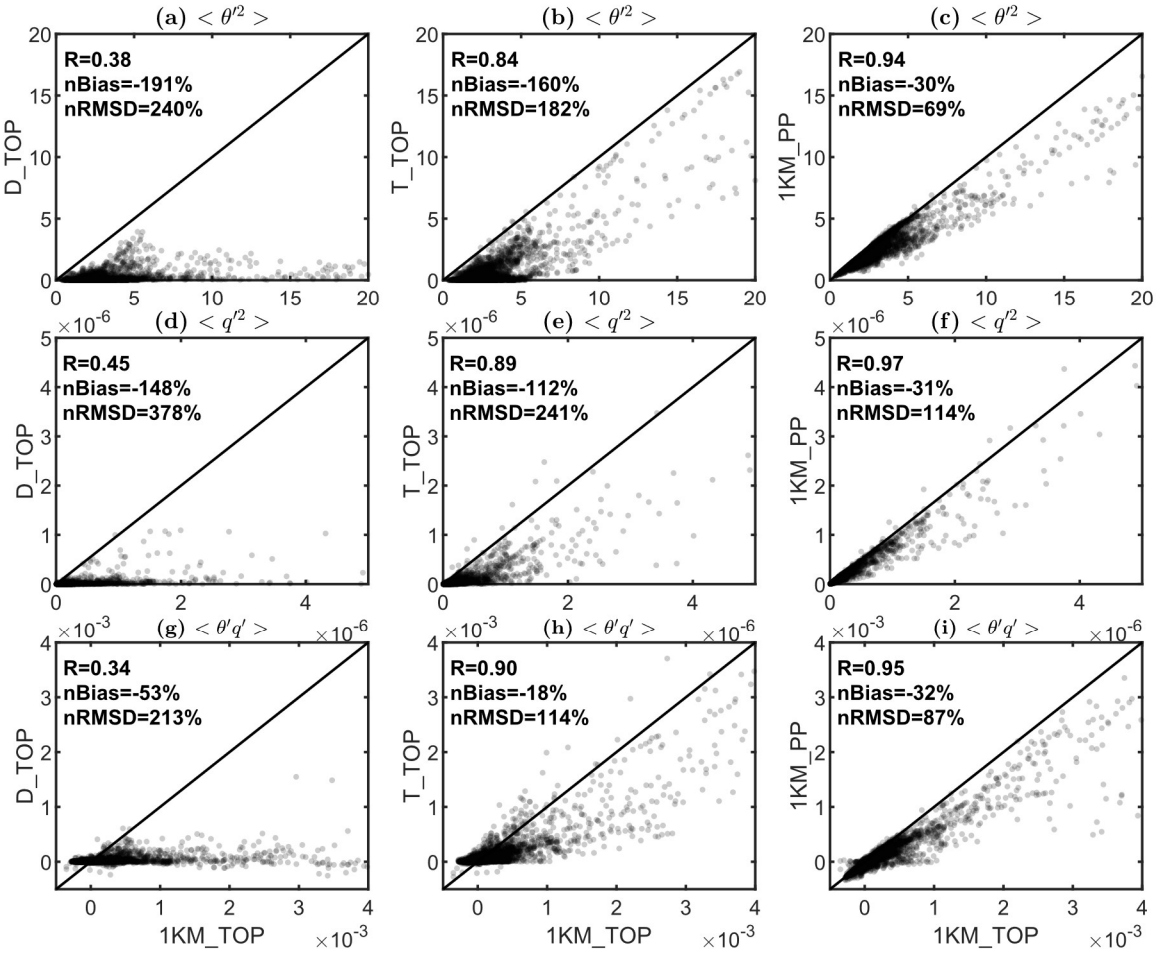

Figure S10. Same as Figure S8, except for G4.

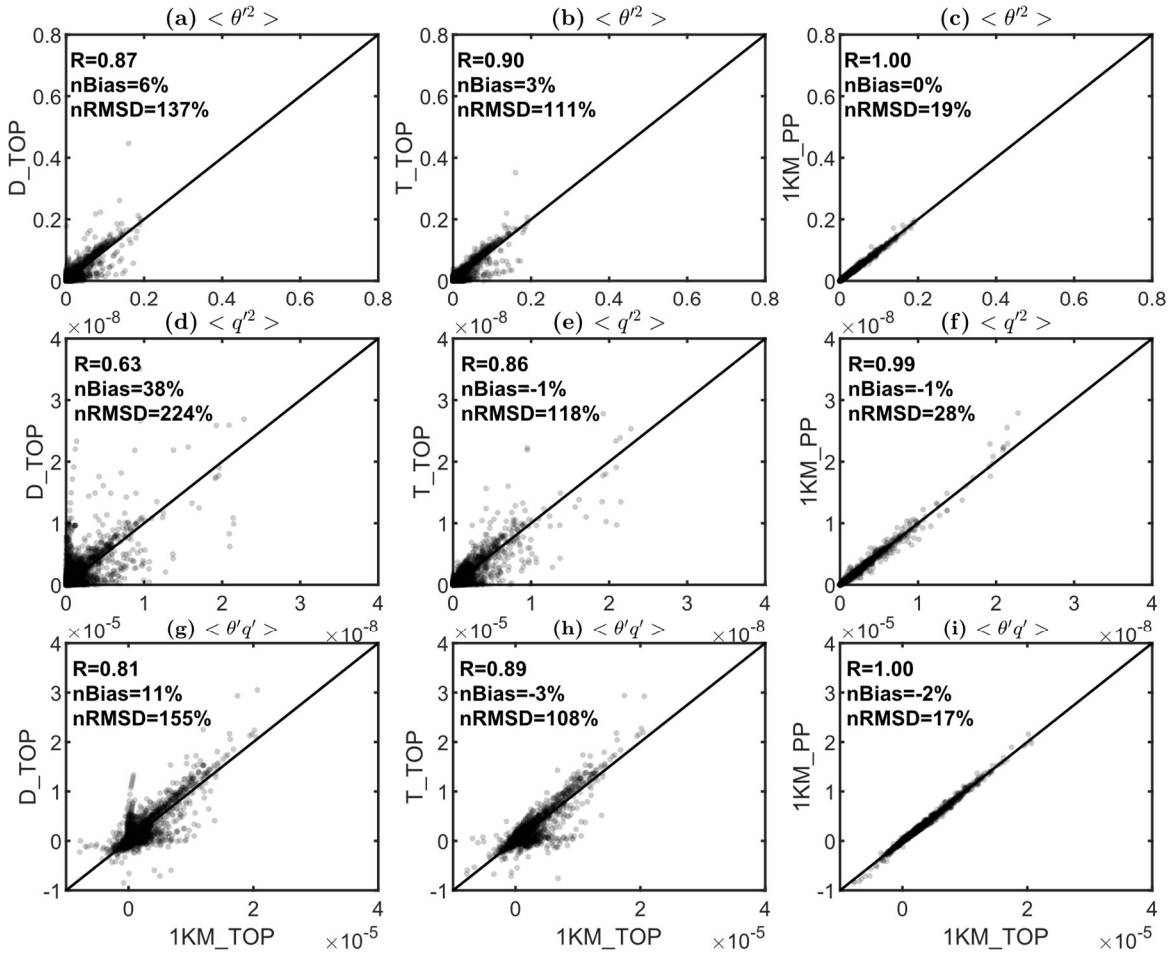

Figure S11. Comparisons of 1KM_TOP simulated (a-c) temperature variance ($\langle\theta'^2\rangle$), (d-e) humidity variance ($\langle q'^2\rangle$), and (g-i) temperature-humidity covariance ($\langle\theta' q'\rangle$) in winter (DJF) over G1 against simulated values from D_TOP , T_TOP and 1KM_PP model configurations. The (co-)variances were derived using the HOM methods introduced in Section 2.4; and R values were shown in each sub-plot.

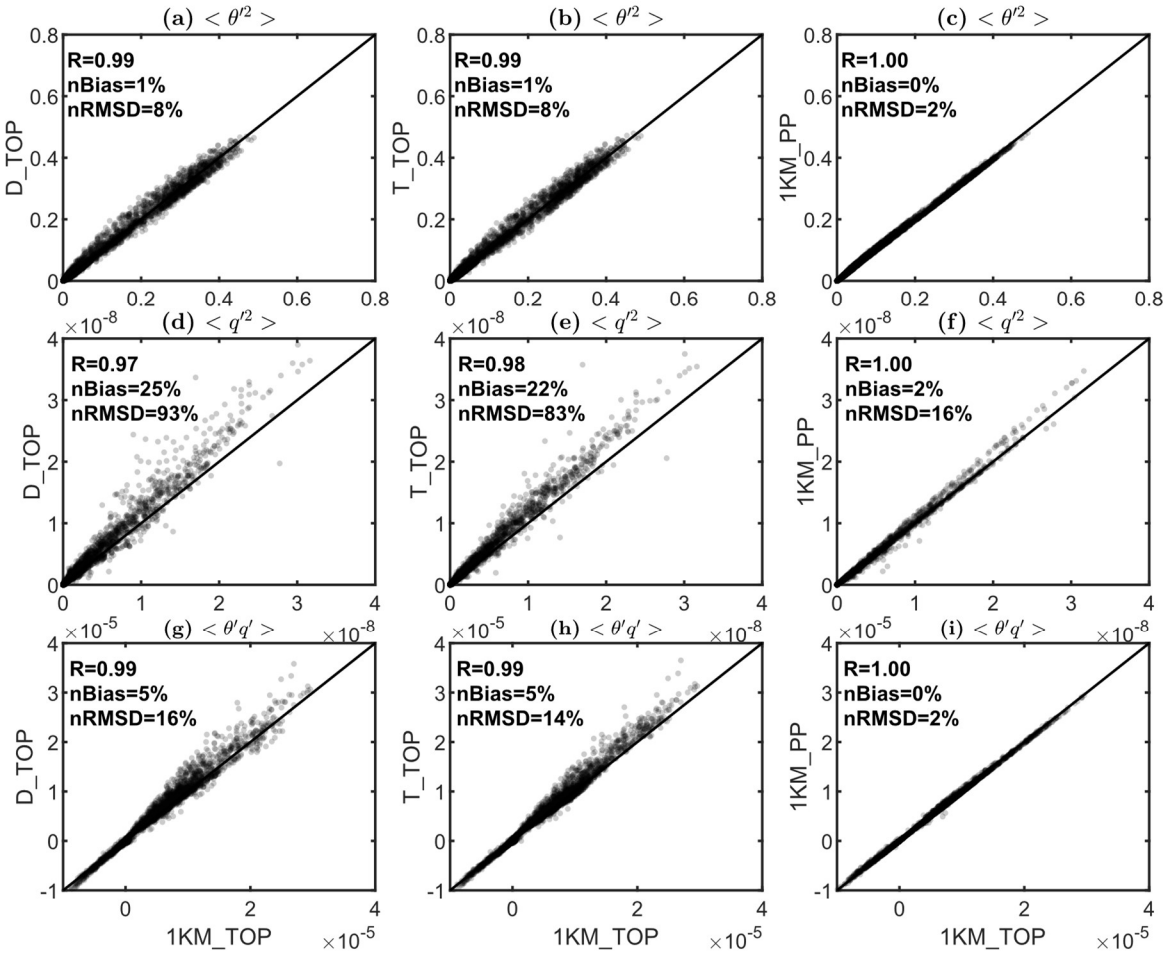

Figure S12. Same as Figure S11, except for summer (JJA).

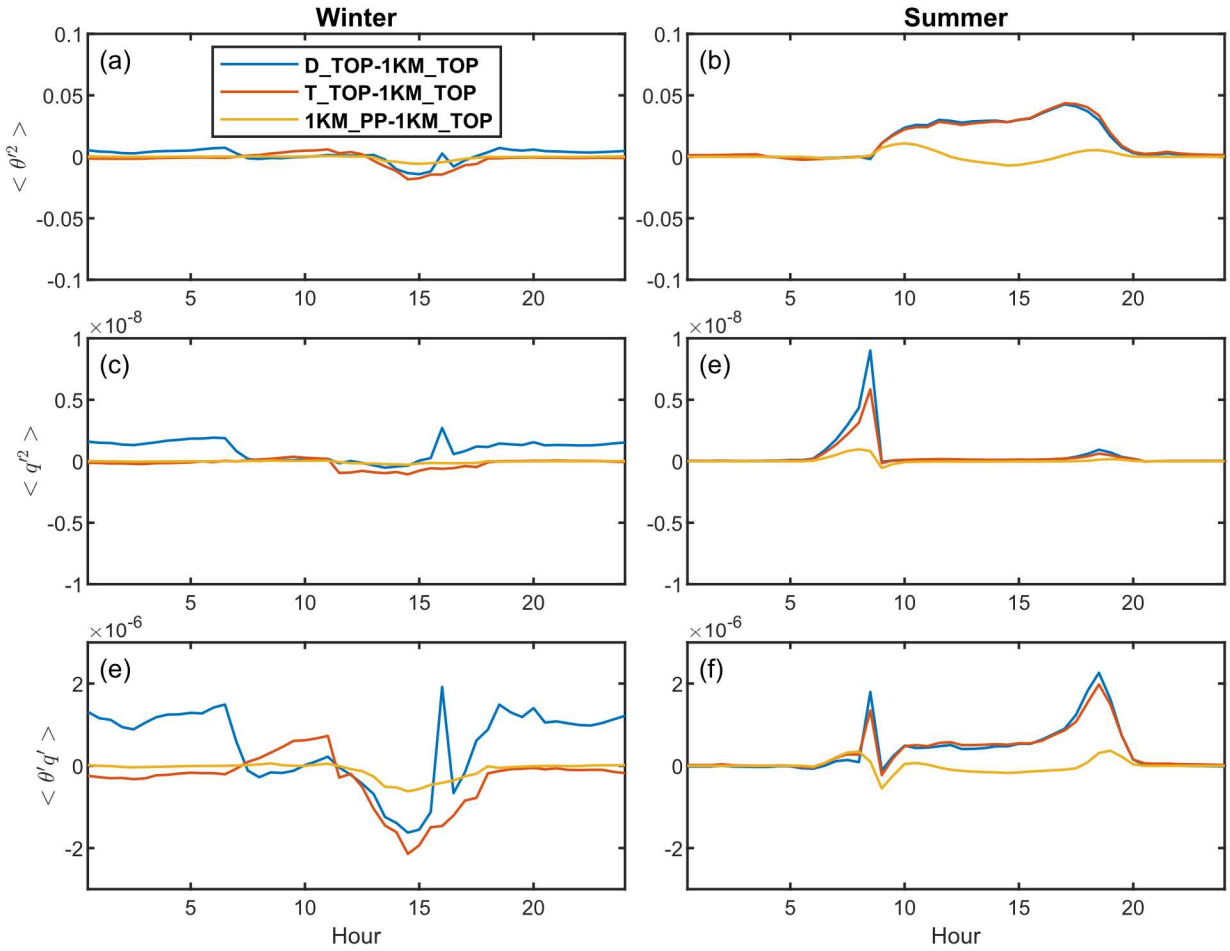

Figure S13. Seasonally-averaged diurnal cycles of the difference in simulated (a-b) temperature variance ($\langle \theta'^2 \rangle$), (c-d) humidity variance ($\langle q'^2 \rangle$), and (e-f) temperature-humidity covariance ($\langle \theta' q' \rangle$) for G1 under different model configurations in winter (DJF) and summer (JJA). Here the local solar time is used and the scalar (co-)variances were derived using the HOM methods introduced in Section 2.4. The differences were calculated as the differences between other cases and 1KM_TOP case.